News for Two-Higgs-Doublet Models

Jack Gunion
U.C. Davis

Pheno 2014, May 6, 2014

The present situation

- **We have now observed a very SM-like Higgs state near $125.5\ \mathrm{GeV}$.**

  The observed mass is very exciting, both experimentally and theoretically, given the large number of production/decay modes in which a signal can be seen and given the fact that $125.5\ \mathrm{GeV}$ is close to being too large for SUSY to "naturally" predict and too small for the SM to be valid all the way to the Planck scale.

  The ongoing order of business is to quantify the observed signal. The observables are various rates that are usually defined relative to the SM:

$$\mu_X^H(Y) = \frac{\sigma^H(X)\mathrm{BR}(H \to Y)}{\sigma^{h_{SM}}(X)\mathrm{BR}(h_{SM} \to Y)} \tag{1}$$

  If we compute C_g and C_γ (relative to the SM values) using only SM loops and take $C_D = C_L$, and $C_W = C_Z \equiv C_V$ as is the case for many models, fitting the $[\mathrm{ggF} + \mathrm{ttH}, \mathrm{VBF} + \mathrm{VH}]$ ellipses in various final states Y $\Rightarrow$:

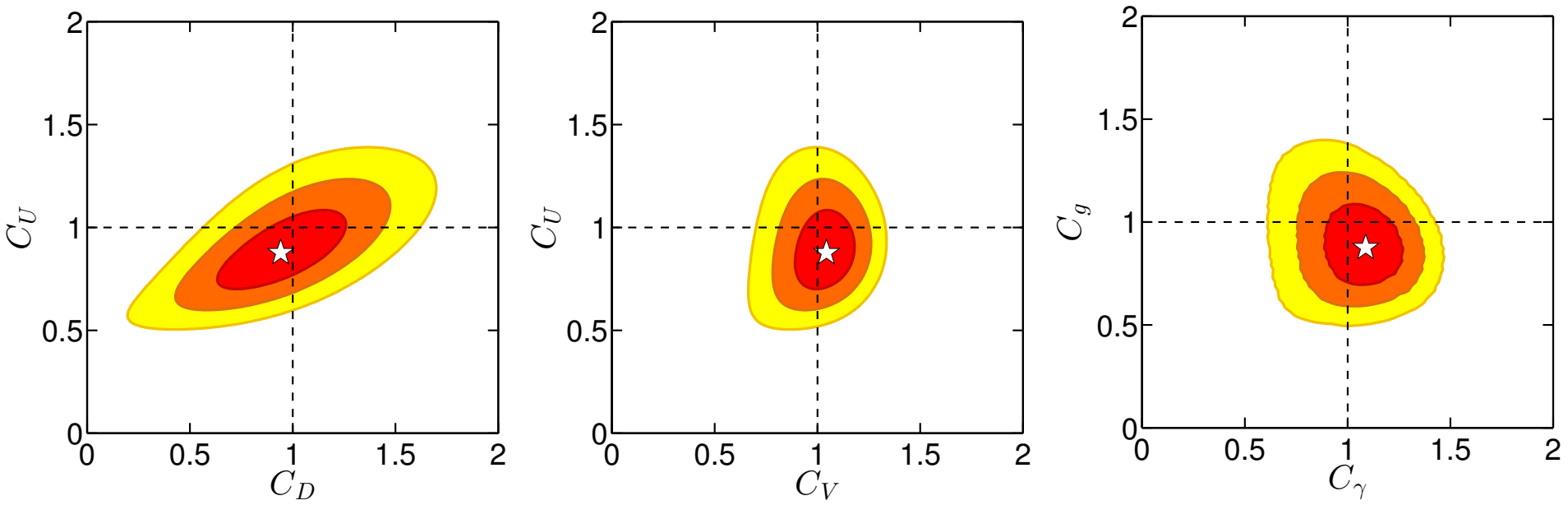

Figure 1: Coupling constant ellipses. The filled red, orange and yellow ellipses show the 68%, 95% and 99.7% CL regions, respectively,. The white stars mark the best-fit points.

Certainly, the SM is doing quite well. Fitting to relative coupling constants for the SM-like Lagrangian, one finds that C_U, C_D, C_V are fully consistent with SM-like values of unity, while extra contributions to the $\gamma\gamma$ and gg loop diagrams are consistent with being absent.

However, this result does not imply that there are no other Higgs bosons.

Other Higgs bosons can be present without disturbing significantly the quality of the fit to the 125.5 GeV data.

- **Given the current data set, heavier or lighter Higgs bosons can have escaped detection due to inadequate cross section.**
- **Lighter Higgs bosons could even be present in the decays of the $125.5\ \mathrm{GeV}$ state.**

- **With regard to the latter, there is the generic possibility of invisible (inv) and/or unseen (U), but not truly invisible, Higgs decays.**

  Invisible decays are now somewhat constrained by searches for ZH production with Z detection in some channel or other and requiring that no tracks etc. are present that could come from the H.

  An overview is given in Fig. 2, which shows the behavior of $\Delta\chi^2$ as a function of $\mathrm{BR}_{\mathrm{inv}}$ for various different cases of interest; in particular note the result:

  C_U, C_D **free,** $C_V \leq 1$**,** $\Delta C_\gamma = \Delta C_g = 0$ **—** $\mathrm{BR}_{\mathrm{inv}} < 0.09$ **(0.24)**
  at 68% **(**95%**) CL.**

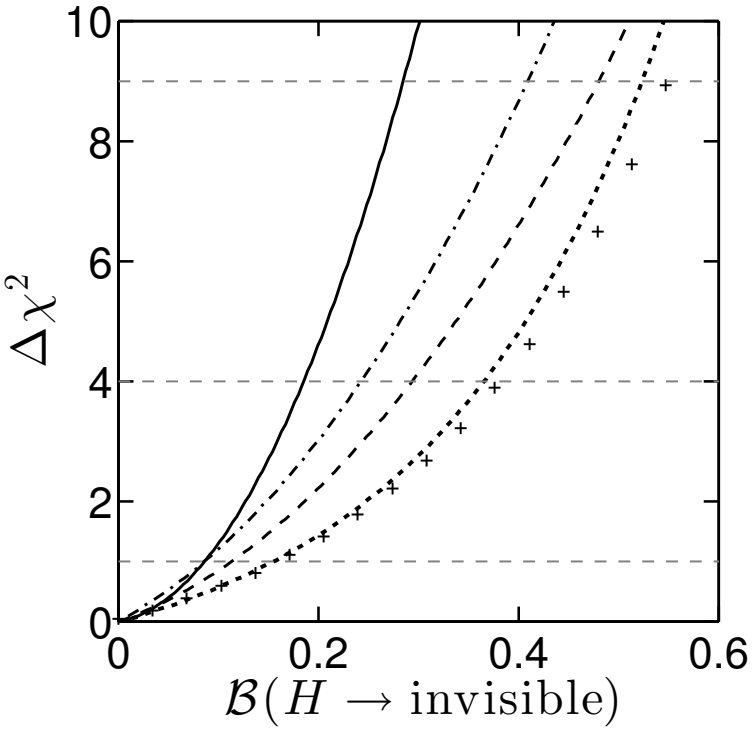

Figure 2: $\Delta\chi^2$ **distributions for the branching ratio of invisible Higgs decays for various cases. Solid: SM+invisible. Dashed: varying** ΔC_g **and** ΔC_γ **for** $C_U = C_D = C_V = 1$**. Dotted: varying** C_U**,** C_D **and** C_V **for** $\Delta C_g = \Delta C_\gamma = 0$**. Dot-dashed: varying** C_U**,** C_D **and** $C_V \leq 1$ **for** $\Delta C_g = \Delta C_\gamma = 0$**. Crosses: varying** C_U**,** C_D**,** C_V**,** ΔC_g **and** ΔC_γ**.**

- **When** $C_V \leq 1$**,** $H \to$ **invisible is much more constrained by the global fits to the** H **properties than by the direct searches for invisible decays,** *cf.* **the solid, dashed and dash-dotted lines in Fig. 2.** $\Rightarrow$ **little change if** $\text{inv} \to U$**, e.g.** $\text{BR}_U \leq 0.39$ **at 95% CL.**

2HDM Models

(Dumont, Gunion, Jiang, Kraml, in preparation)

- **The most general 2HDM Higgs potential is given by**

$$
\begin{aligned}
V &= m_1^2|H_1|^2 + m_2^2|H_2|^2 + \frac{\lambda_1}{2}|H_1|^2 + \frac{\lambda_2}{2}|H_2|^2 + \lambda_3|H_1|^2|H_2|^2 \\
&\quad +\lambda_4|H_1^\dagger H_2|^2 + \frac{\lambda_5}{2}\left((H_1H_2)^2 + \text{c.c.}\right) + m_{12}^2\left(H_1H_2 + \text{c.c.}\right) \\
&\quad + \left(\lambda_6|H_1|^2(H_1H_2) + \text{c.c.}\right) + \left(\lambda_7|H_2|^2(H_1H_2) + \text{c.c.}\right) \ .
\end{aligned} \tag{2}
$$

The terms involving λ_6 and λ_7 represent a hard breaking of the Z_2 symmetry that is used to avoid excessive FCNC, so set them to 0. We also assume no CP violation, $i.e.$ all parameters are taken to be real.

Various different ways of specifying the parameters are possible. The most direct way is to specify the λ_i. But, for our purposes, it is best to determine

the λ_i in terms of the parameter set

$$m_h, \quad m_H, \quad m_{H^\pm}, \quad m_A, \quad \tan\beta, \quad m_{12}^2, \quad \alpha\,, \tag{3}$$

with $\beta \in [0, \pi/2]$, $\alpha \in [-\pi/2, +\pi/2]$; m_{12}^2 (the parameter that softly breaks the Z_2 symmetry) can have either sign.

The two simplest models are called Type-I and Type-II with fermion couplings as given in the table.

	Type I and II	Type I		Type II	
Higgs	C_V	C_U	C_D	C_U	C_D
h	$\sin(\beta-\alpha)$	$\cos\alpha/\sin\beta$	$\cos\alpha/\sin\beta$	$\cos\alpha/\sin\beta$	$-\sin\alpha/\cos\beta$
H	$\cos(\beta-\alpha)$	$\sin\alpha/\sin\beta$	$\sin\alpha/\sin\beta$	$\sin\alpha/\sin\beta$	$\cos\alpha/\cos\beta$
A	**0**	$\cot\beta$	$-\cot\beta$	$\cot\beta$	$\tan\beta$

Table 1: **Tree-level vector boson couplings C_V ($V = W, Z$) and fermionic couplings C_F ($F = U, D$) normalized to their SM values for the Type I and Type II Two-Higgs-Doublet models.**

- **Either the h or the H can be SM-like with mass ~ 125.5 GeV, labelled $h125$ and $H125$, respectively.**

- **Proceed in steps:**

1. **Choose $h125$ or $H125$.**
2. **Scan:**

$$\alpha \in [-\pi/2, +\pi/2]\,, \quad \tan\beta \in [0.5, 60]\,, \quad m_{12}^2 \in [-(2\ \text{TeV})^2, (2\ \text{TeV})^2]\,,$$
$$m_A \in [5\ \text{GeV}, 2\ \text{TeV}]\,, \quad m_{H^\pm} \in [m^*, 2\ \text{TeV}]\,, \tag{4}$$

   where m^* is the lowest value of $m_{H^\pm}$ allowed by LEP direct production limits and B physics constraints.
3. **Apply all constraints from preLHC (B-physics, LEP limits, ...)**
4. **Impose LHC limits on Higgs bosons heavier than 125.5 GeV (H and A in the $h125$ case, or just A in the $H125$ case).**
5. **Impose Higgs fitting for all channels as per arXiv:1306.2941 (Beranger, et.al.) at the 95% CL.**
6. **New: Require that feed down (FD) from heavier Higgs bosons not disturb the 125 GeV fits. e.g. for the $h125$ case the most important channels are: $gg \to H \to hh$ and $gg \to Z \to Zh$.**
7. **Look at consequences.**

The $h125$ case

- **Note: $|\alpha| \leq \pi/2$ implies that $C_U^h = C_D^h > 0$ for Type I, whereas for Type II $C_D^h < 0$ is possible when $\sin\alpha > 0$.**

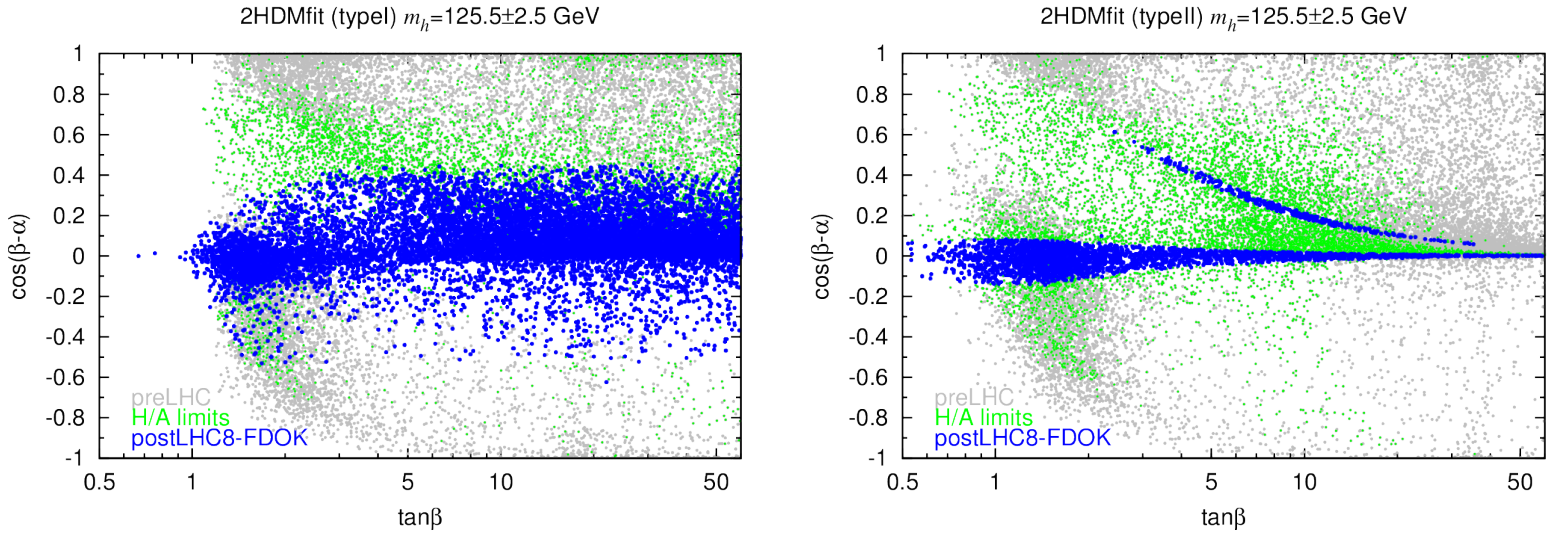

Figure 3: **Constraints in the $\cos(\beta-\alpha)$ versus $\tan\beta$ for $m_h \sim 125.5$ GeV. Grey points satisfy preLHC constraints, while green points satisfy in addition the LHC limits on H and A production. Blue points fall in addition within the 7+8 TeV 95% CL ellipses in the $[\mu(\mathrm{ggF}+\mathrm{ttH}), \mu(\mathrm{VBF}+\mathrm{VH})]$ plane for each of the final states considered, $Y = \gamma\gamma, ZZ, WW, b\bar{b}, \tau\tau$.**

The SM limit is $\cos(\beta-\alpha)\to 0$. For Type II there is a main branch that is very SM-like, but also an alternative branch that is quite different. This is a branch having $C_D^h\sim -1$. The future LHC run can eliminate or confirm this branch — more later. (arXiv:1403.4736, Ferreira, et. al.)

- **What masses are possible for the heavy H and, possibly, A?**

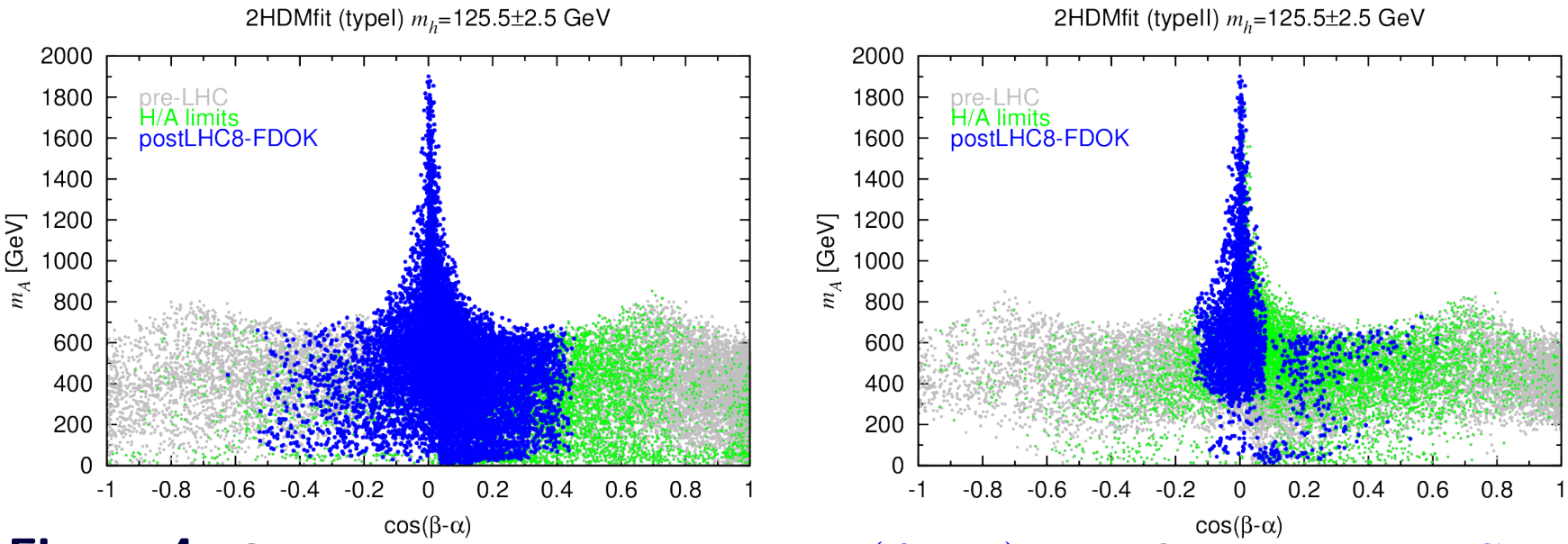

Figure 4: Constraints in the m_A versus $\cos(\beta-\alpha)$ plane for $m_h\sim 125.5$ GeV.

The decoupling limit is clearly seen. The Type-II high $\cos(\beta-\alpha)>0$ points are those with $C_D^h\sim -1$.

- **Could the A be hiding in current data? YES! At low m_A, very large $gg \to A$ and bbA, $A \to \tau\tau$ rates are possible in Type II.**

  Key point: CMS limits for $m_A \lesssim 100$ GeV are a bit weak and only go down to 90 GeV, while LEP limits from $Z^* \to hA$ are evaded because of small ZhA coupling ($\propto \cos(\beta - \alpha)$) when h is SM-like.

- **Implications for the future**

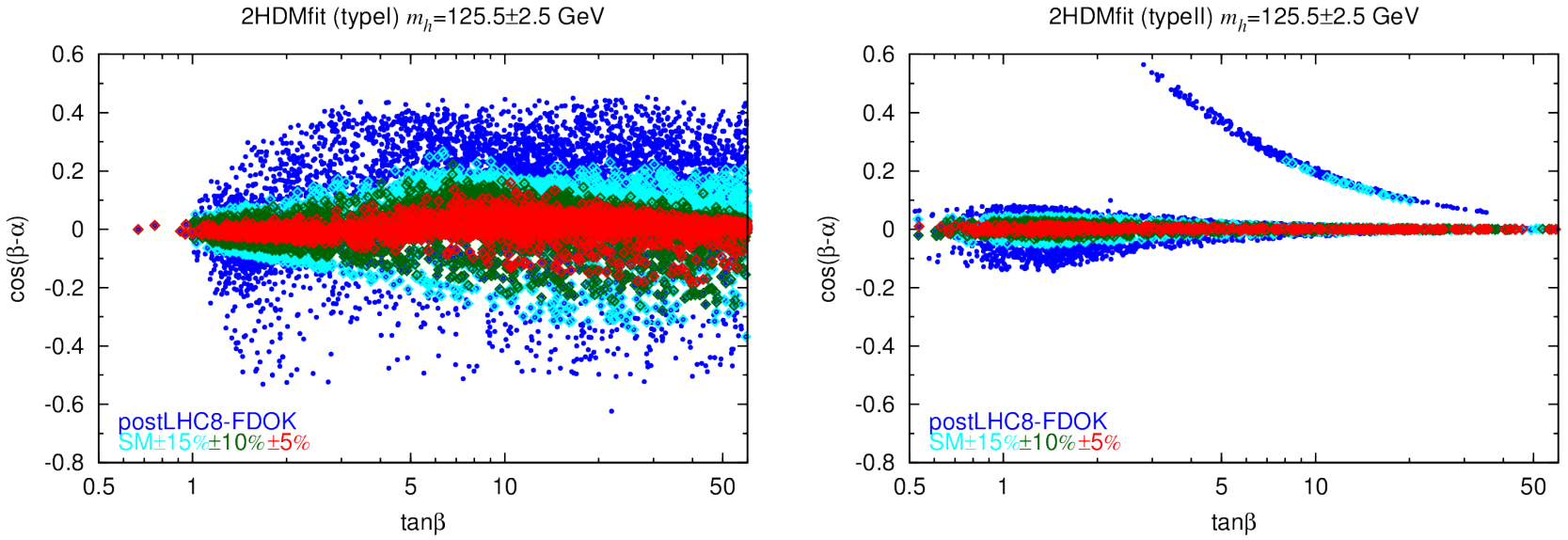

Figure 5: postLHC8-FDOK points in the $\cos(\beta - \alpha)$ vs. $\tan\beta$ plane for the $h125$ scenario comparing current h fits (blue) to the case that the rates for all the channels listed below are within $\pm 15\%$ (cyan), $\pm 10\%$ (green) or $\pm 5\%$ (red) of the SM Higgs prediction.

$$(X, Y) = (gg, \gamma\gamma),\ (gg, ZZ),\ (gg, \tau\tau),\ (\mathrm{VBF}, \gamma\gamma),\ (\mathrm{VBF}, ZZ),\ (\mathrm{VBF}, \tau\tau) = (\mathrm{VH}, bb),\ (\mathrm{ttH}, bb)\,.$$

Note that even SM$\pm 10\%$ ($\sim L = 300$ fb^{-1} at 14 TeV) on each of the individual μ's will have eliminated the "wrong-sign" down-quark Yukawa region (which corresponds to $\sin\alpha > 0$ or $C_D^h < 0$) of the Type II model.

Looking forward, LHC and ILC will measure $C_{hhh} \equiv \lambda_{hhh}/\lambda_{hhh}^{\rm SM}$. We find:

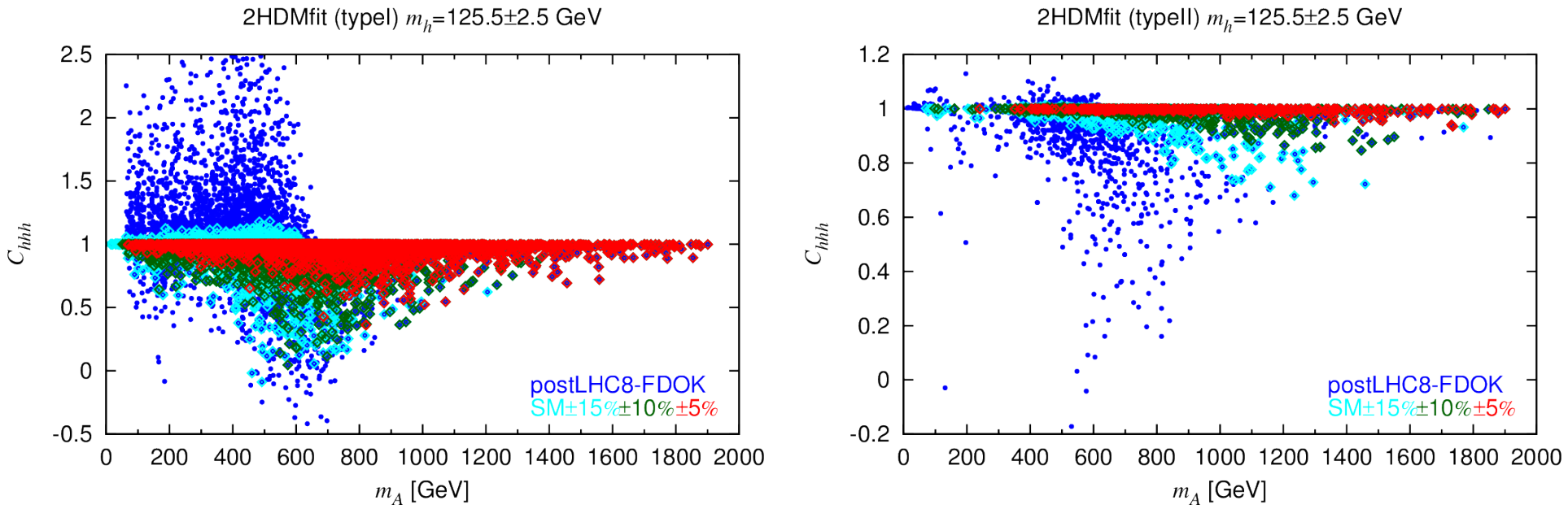

Figure 6: postLHC8-FDOK points in the C_{hhh} vs. m_A plane for the $h125$ scenario comparing current h fits to the $\pm 15\%, \pm 10\%, \pm 5\%$ possibilities; FDOK is required in all cases. Color scheme is as for Fig. 6.

- **Thus, $\mu_X(Y)$ excursions from unity at the currently allowed 95% level extreme, $\Rightarrow$ observation of a large deviation from $C_{hhh} = 1$ would be quite likely.**
  For example, at the high-luminosity LHC14, with $L = 3000$ fb^{-1} one can measure C_{hhh} to the 50% level, and deviations of this order, indeed up to 100% or more, are possible.
- **However, if future LHC measurements approach the SM then observing a deviation from $C_{hhh} = 1$ becomes increasingly difficult, even at the ILC.**
- **The predicted precision on λ_{hhh} for ILC1000 with $L = 500 - 1000$ fb^{-1} is of order 21% and for ILC1000 with $L = 1600 - 2500$ fb^{-1} is of order 13%. At CLIC3000 with $L = 2000$ fb^{-1} the accuracy achievable would be about 10%.**
- **In Type I, SM$\pm 10\%$ still allows C_{hhh} as small as ~ 0, while SM$\pm 5\%$ allows C_{hhh} as small as 0.3, either of which will be observable for any of the listed machines and integrated L values.**
  In contrast, for Type II, the smallest C_{hhh} for SM$\pm 10\%$ is ~ 0.9, while for SM$\pm 5\%$ it is ~ 0.95.
  The former would require CLIC3000 while the latter would be beyond

the reach of any of the above e^+e^- colliders.

$\sqrt{s} = 14$ TeV Results for ggFH, A+bbH, A production in the $\tau\tau$ final state are displayed in Fig. 8.

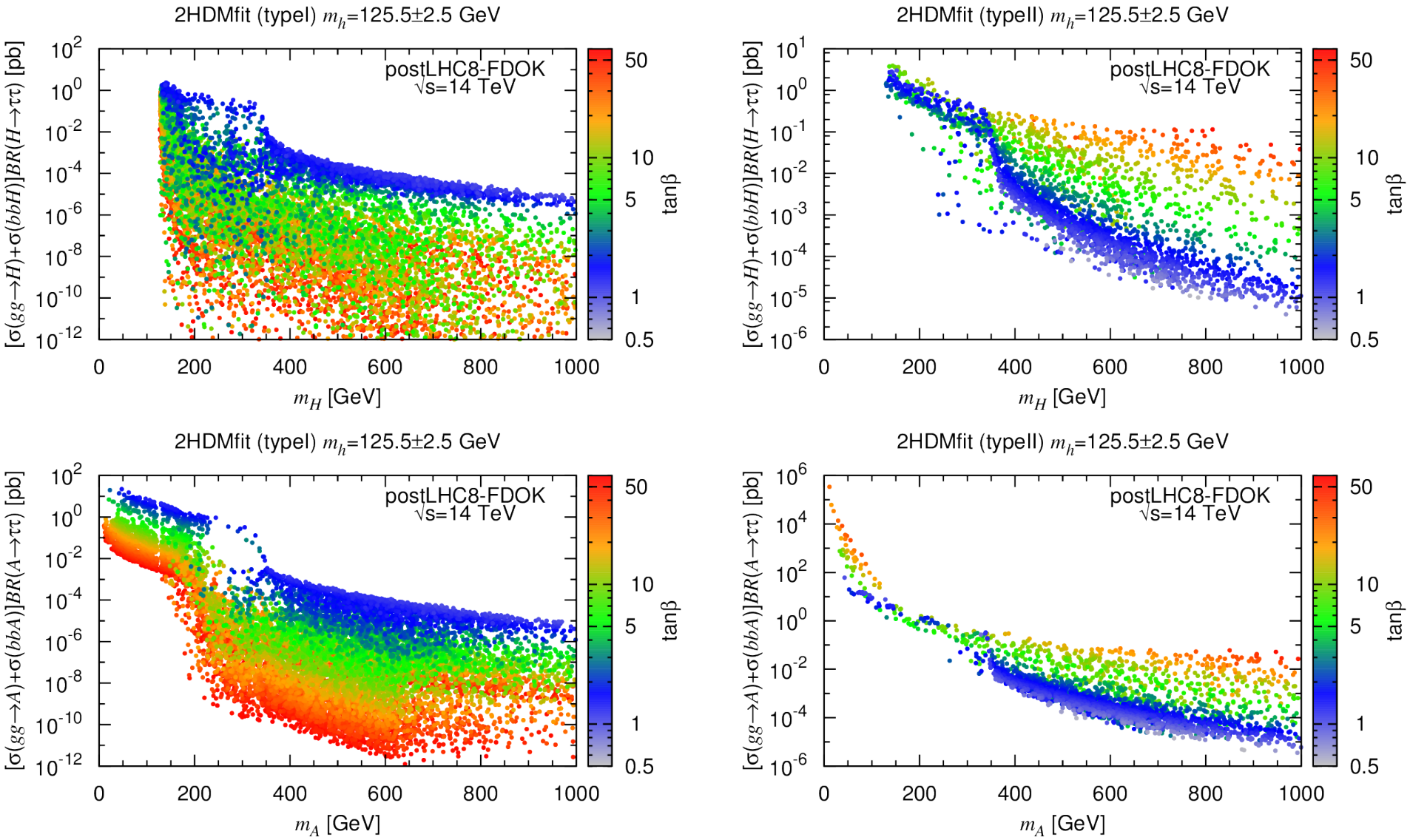

Figure 7: $[\sigma(gg \to H) + \sigma(bbH)]\mathrm{BR}(H \to \tau\tau)$ **and** $[\sigma(gg \to A) + \sigma(bbA)]\mathrm{BR}(A \to \tau\tau)$ **in pb as functions of** m_H **(top row) and** m_A **(bottom row), for postLHC8-FDOK points with** $m_h \sim 125.5$ GeV**. The values of** $\tan\beta$ **are color-coded as indicated on the plots.**

- **Overall, the range of possible cross sections is quite large.**
- **For Type I, maximum values are of order $1 - 10$ pb and minimum values below 10^{-10} pb (although this range is somewhat narrowed on average as the h is required to be more and more SM-like).**
- **For Type II, minimum values are of order $10^{-4} - 10^{-5}$ pb and maximum values at low mass, esp. low m_A are very large.**
  (Few points survive below $m_H \sim 300$ GeV if the 125.5 GeV state rates lie within 5% of the SM Higgs predictions.)
- **An alternative view is in the $\tan\beta$ vs. m_A plane, Fig. 9.**
  Note the high σBR points at low m_A that escape all limits and fall outside the usual "wedge". Surely, LHC Run2 analyses can be designed that will eliminate this region despite the manifest experimental difficulties associated with $\tau\tau$ masses below and near 90 GeV.
  We also see that if we can probe to $\sigma\mathrm{BR} \gtrsim 10^{-2}$ (which we should be able to do at LHC Run2), then most of the normal wedge will be eliminated (or something seen) for $m_A \lesssim 500$ GeV.
- **Don't forget the $\mu\mu$ final state with rates obtained by multiplying by $\mathrm{BR}(\mu\mu)/\mathrm{BR}(\tau\tau) \sim 3.5 \times 10^{-3}$.**

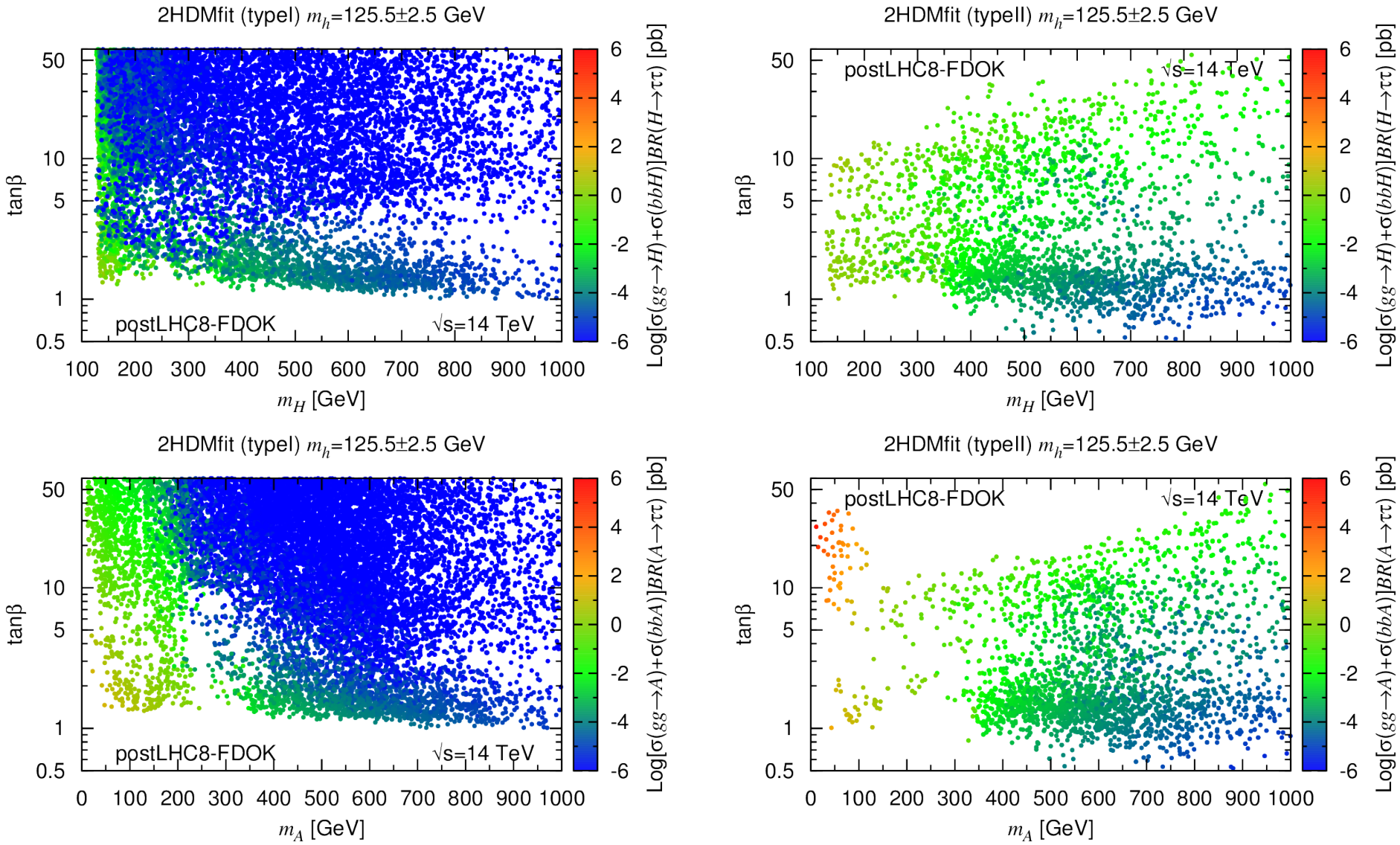

Figure 8: Same information as in Fig. 8 but in the $\tan\beta$ vs. m_H (top row) and $\tan\beta$ vs. m_A (bottom row) planes with the cross section color-coded as indicated by the scales on the right of the plots. Only FDOK points are shown.

Also, rates in the $\gamma\gamma$ final state can be at an interesting level.

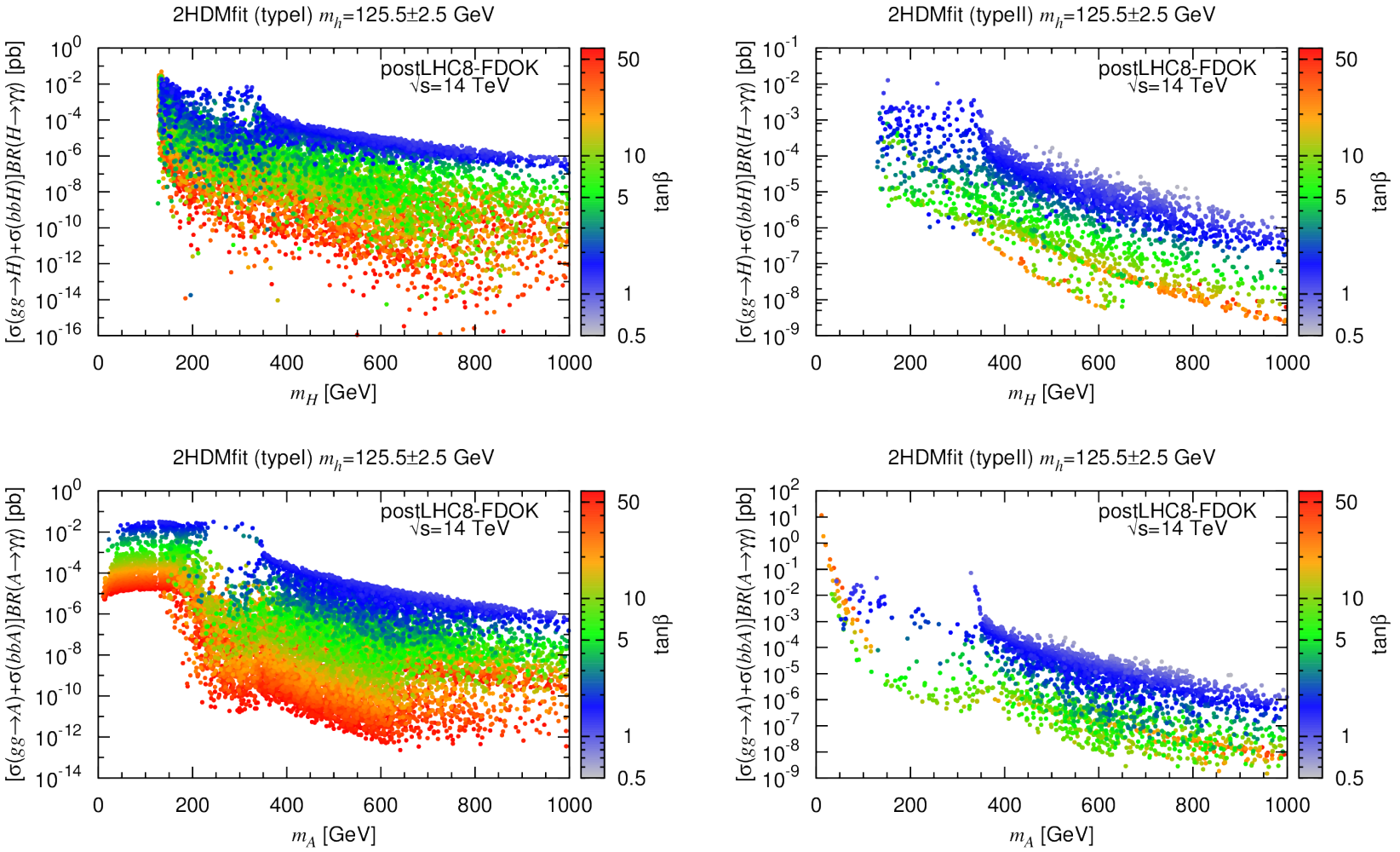

Figure 9: $[\sigma(gg \to H) + \sigma(bbH)]\mathrm{BR}(H \to \gamma\gamma)$ **and** $[\sigma(gg \to A) + \sigma(bbA)]\mathrm{BR}(A \to \gamma\gamma)$ **in pb as functions of** m_H **(top row) and** m_A **(bottom row), for postLHC8-FDOK points with** $m_h \sim 125.5$ GeV**. The values of** $\tan\beta$ **are color-coded as indicated on the plots.**

Of course, once m_A or m_H is above the ZZ and $t\bar{t}$ thresholds, the rates in the ZZ and $t\bar{t}$ final states will be of great interest. The former (latter) are shown in Fig. 11(Fig 12).

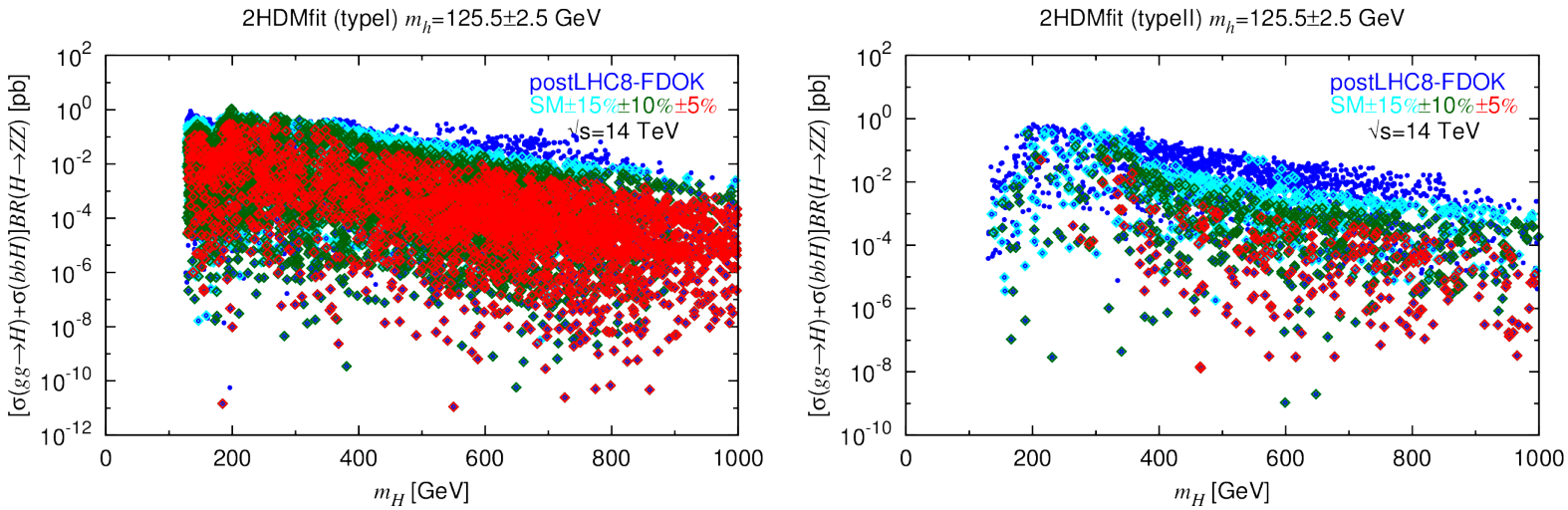

Figure 10: We plot $[\sigma(gg \to H) + \sigma(bbH)]\mathrm{BR}(H \to ZZ)$. Implications of various levels of precision for future h measurements are displayed.

ZZ rates are suppressed with increasingly SM-like $h125$.

In $t\bar{t}$, large $\sigma \times \mathrm{BR}$ values are certainly possible, but so also are very small values, although in the case of Type II the smallest values found at m_H or m_A of order 1 TeV is $\sim 10^{-4}$ pb.

This latter might be detectable for full Run2 luminosity of $L = 300$ fb^{-1},

and is certainly of great interest for the high-luminosity run of the LHC which might accumulate $L = 3000\ \mathrm{fb}^{-1}$.

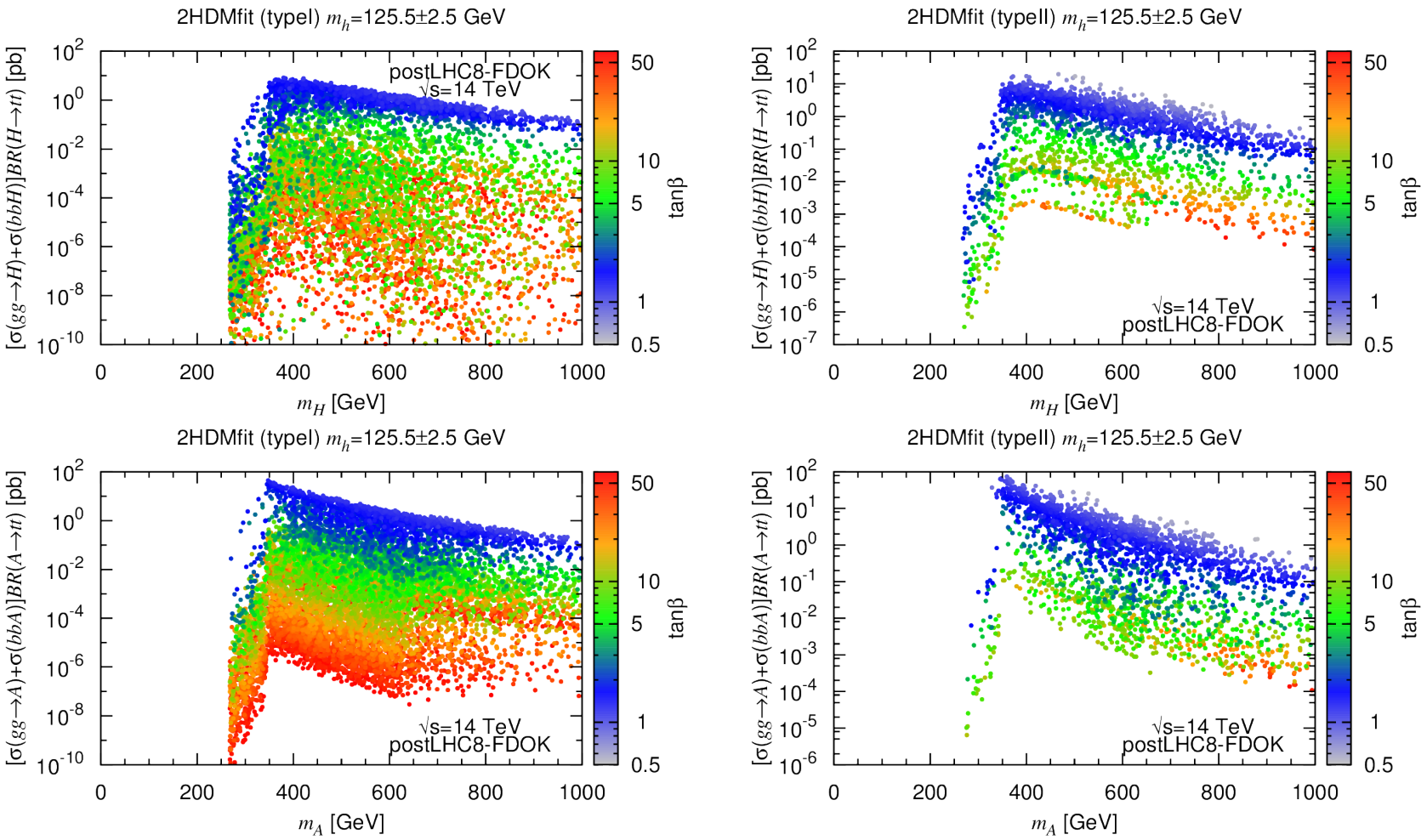

Figure 11: We plot $[\sigma(gg \to H) + \sigma(bbH)]\mathrm{BR}(H \to t\bar{t})$ and $[\sigma(gg \to A) + \sigma(bbA)]\mathrm{BR}(A \to t\bar{t})$.

- **Wrong-sign C_D^h and charged Higgs non-decoupling**

  The $C_D^h \sim -1$ Type II wing is eliminated if the h is measured to be sufficiently SM-like.

  It will also be eliminated or confirmed with sufficiently precise measurements at the ILC.

  The crucial ingredients are deviations in $\kappa_g^2 \equiv \Gamma(h \to gg)/\Gamma_{\rm SM}(h \to gg)$ and κ_γ^2. $\kappa_\gamma \sim 0.95$ as a result of a non-decoupling charged Higgs boson loop contribution to $h \to \gamma\gamma$. $\kappa_g \sim 1.13$ due to the change in the top-bottom loop interference. (I use Ferreira et. al notation. $C_g^h = \kappa_g$, $C_\gamma^h = \kappa_\gamma$)

  – **According to the recent Snowmass studies, the LHC can measure κ_g to 6–8% for $L = 300$ fb^{-1} and 3–5% for $L = 3000$ fb^{-1}, based on fitting all the rates rather than directly observing the gg final state.**
  At the ILC, $e^+e^- \to Z^* \to Zh$ determines the ZZh coupling very accurately and isolation of the gg final state is easier. The error on κ_g estimated is 2% for a combination of $L = 250$ fb^{-1} at $\sqrt{s} = 250$ GeV and $L = 500$ fb^{-1} at $\sqrt{s} = 500$ GeV.

Thus, both the LHC and ILC will be able to determine whether or not C_D^h is positive using the indirect fit and direct measurement of κ_g, respectively.

- **The 5% suppression of κ_γ for $C_D^h < 0$ should be measurable at the $\sqrt{s} = 14$ TeV LHC run for $L = 3000$ fb^{-1}.**
  At the ILC, for a combination of $L = 250$ fb^{-1} at $\sqrt{s} = 250$ GeV and $L = 500$ fb^{-1} at $\sqrt{s} = 500$ GeV the expected error on κ_γ is $\sim 8.3\%$ (including a 0.5% theory uncertainty) based on measuring $e^+e^- \to Zh$ with $h \to \gamma\gamma$, implying that the sign of C_D^h cannot be directly determined at the ILC using the $\gamma\gamma$ final state.

- **Let's explore further the charged-Higgs non-decoupling. (arXiv:1403.4736, Ferreira, et. al.)**

  In figures, the notations $\kappa_d = C_D^h$, etc. are employed.

  First, it is easily seen that C_D^h is negative when $\sin(\beta + \alpha) \sim 1$, i.e. not the usual $\sin(\beta - \alpha) \sim 1$ decoupling limit.

In this case, the relative hVV and hhh couplings satisfy

$$C_V^h, C_{hhh} \to (\tan^2\beta - 1)/(\tan^2\beta + 1) \quad (\sin(\beta+\alpha) \to 1). \tag{5}$$

$\Rightarrow$ at large $\tan\beta$ can't use either C_V^h or C_{hhh} to rule out wrong sign case.

We performed a scan very similar to that already discussed. After passing all preLHC constraints, the points were used to calculate the various $\mu_X^h(Y)$.

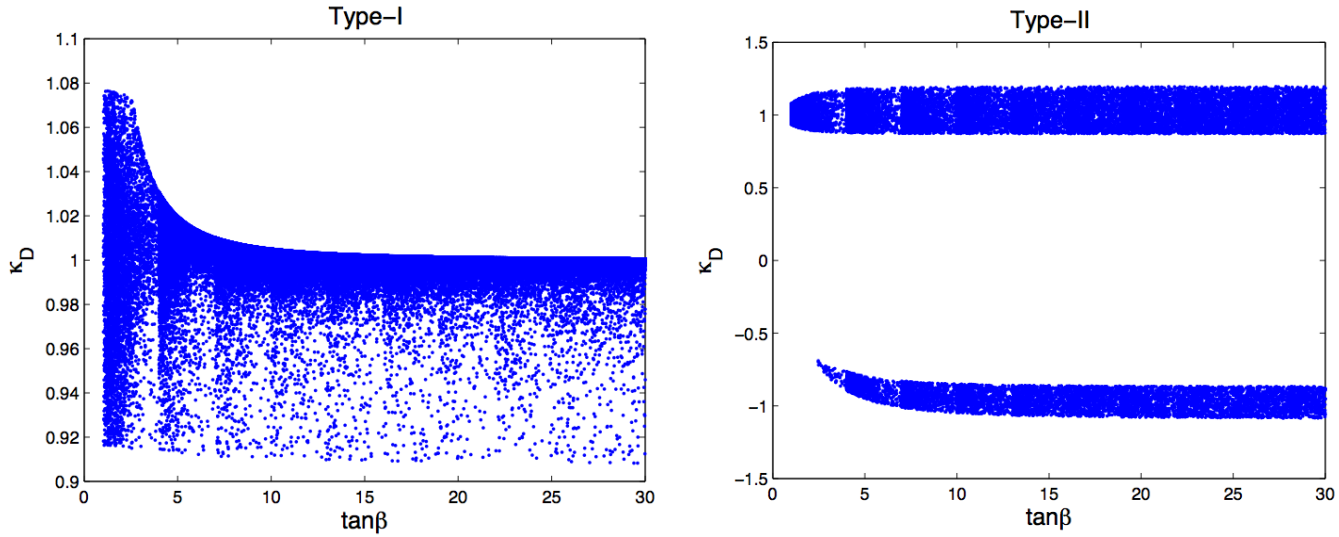

Figure 12: Ratio of the lightest Higgs couplings to down quarks in the 2HDM relative to the SM as a function of $\tan\beta$. Left - Type-I and right - Type-II. All μ's required to be within 20% of the SM value.

In Fig. 13 we show $\kappa_d \equiv C_D^h$ in Type-I and Type-II models as a function of $\tan\beta$ for those parameter space points that pass all theoretical and experimental constraints and have all $\mu_X^h(Y)$'s within 20% of the SM prediction of 1. The two regions with opposite sign for κ_d are apparent.

If we increase the precision required for the $\mu_X^h(Y)$s, we find

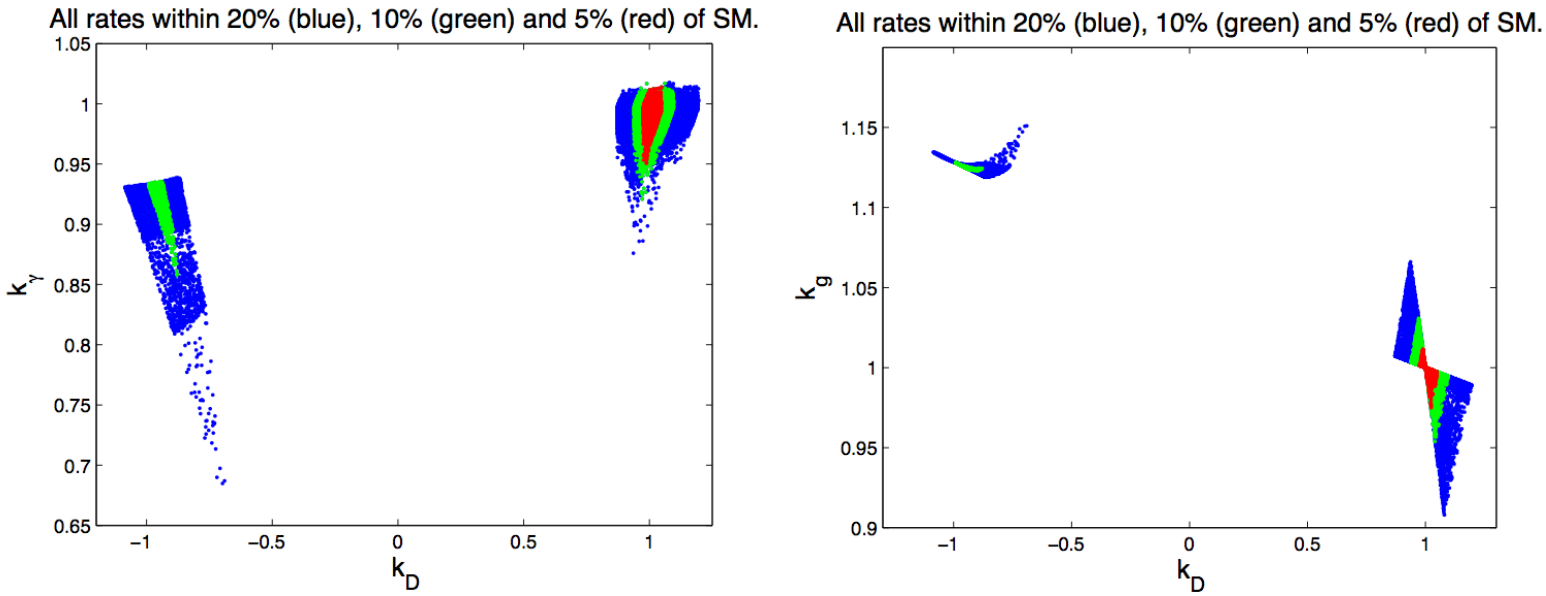

Figure 13: Allowed regions for 2HDM Type-II with all $\mu_X^h(Y)$ within 20% (blue/black), 10% (green/light grey) and 5% (red/dark grey) of their SM values in: Left — κ_γ vs. κ_d space; Right — κ_g vs. κ_d space.

To understand the κ_γ upper limit in the $\kappa_d < 0$ case, we note that the hH^+H^- coupling has the form (JFG+Haber, decoupling) $g_{hH^+H^-} =$:

$$\frac{(2m_A^2 - 2m_{H^\pm}^2 - m_h^2)\sin(\beta-\alpha)\sin\beta\cos\beta + (m_A^2 - m_h^2)\cos 2\beta\cos(\beta-\alpha) + \lambda_5 v^2\cos(\beta+\alpha)}{v^2\sin\beta\cos\beta}. \tag{6}$$

In the decoupling limit, we have $\sin(\beta-\alpha)\to 1$, $\cos(\beta-\alpha)\to 0$, and $m_A^2 \sim m_H^2 \sim m_{H^\pm}^2 \gg v^2$ and $g_{hH^+H^-} \propto v^2/m_{H^\pm}^2$ as follows:

- **The first term inside the brackets of eq. (6) is of order v^2 because of the mass relations (keeping the λ_i perturbative) and the second term is of order v^2 because $\cos(\beta-\alpha) \propto v^2/m_A^2$.**
- **To discuss the third term we need to note that for $\sin(\beta-\alpha)\to 1$ we have $\alpha \to \beta - \pi/2$.**
  Then, term 3 $\to 2v^2\lambda_5$ since $\cos(\beta+\alpha)\to \sin 2\beta = 2\sin\beta\cos\beta$.
- **The net result is that $g_{hH^+H^-}$ is not growing with the Higgs mass squared and so the charged Higgs loop contribution to the $h\to\gamma\gamma$ amplitude is suppressed by a factor of $m_W^2/m_{H^\pm}^2$ relative to the W and t and b loops. This agrees with the idea that a heavy particle that does not acquire mass from the Higgs vev should decouple.**

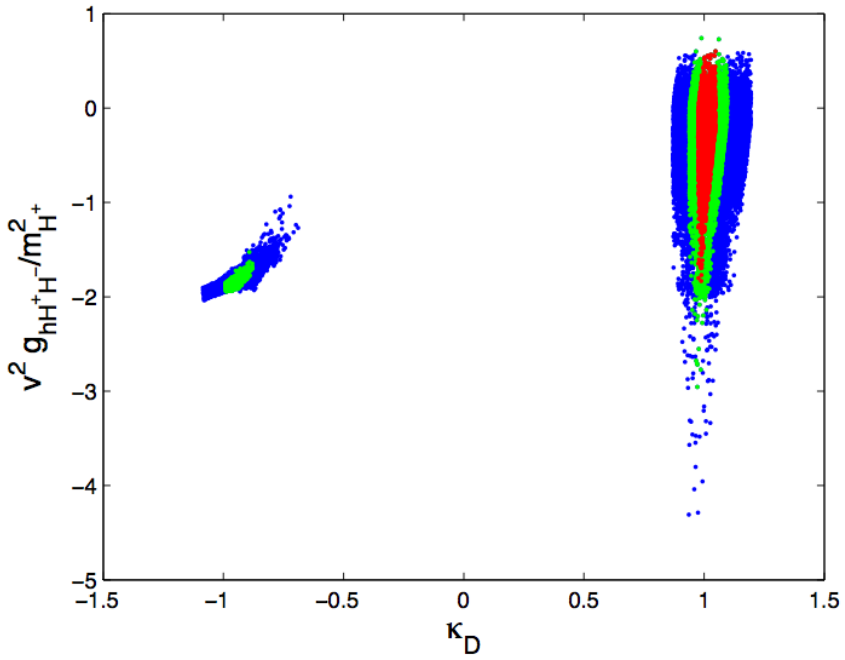

Figure 14: **We show points in the $v^2 g_{hH^+H^-}/m^2_{H^\pm}$ vs. κ_d plane.**

However, the situation is *necessarily* quite different in the case of $\kappa_d < 0$, where $\sin(\beta+\alpha) \to 1$, implying $\alpha \to \pi/2-\beta$. In this limit, $\cos(\beta-\alpha) \to \sin 2\beta$ so that the second term in the numerator of eq. (6) is approximated by $2(m_A^2 - m_h^2)\cos 2\beta$ which approaches $\sim 2m^2_{H^\pm}\cos 2\beta$ as $m_A^2 \sim m_H^2 \sim m^2_{H^\pm} \to \infty$ (at fixed $m_h \sim 125$ GeV). Of course, if $\tan\beta$ is large then $\cos 2\beta \to -1$. Thus, we see from eq. (6) that for $\kappa_d < 0$ we have

$$\frac{v^2 g_{hH^+H^-}}{m^2_{H^\pm}} \sim -2\,, \tag{7}$$

i.e. the $H^\pm$ loop contribution to the $h \to \gamma\gamma$ amplitude will never decouple: -2 corresponds to $\kappa_\gamma \simeq 0.95$.

Of course, there are limits on the maximum $m_{H^\pm}$ deriving from unitarity of the partial wave scattering amplitudes. The strongest constraint comes from a certain eigenamplitude denoted $|a^+|$.

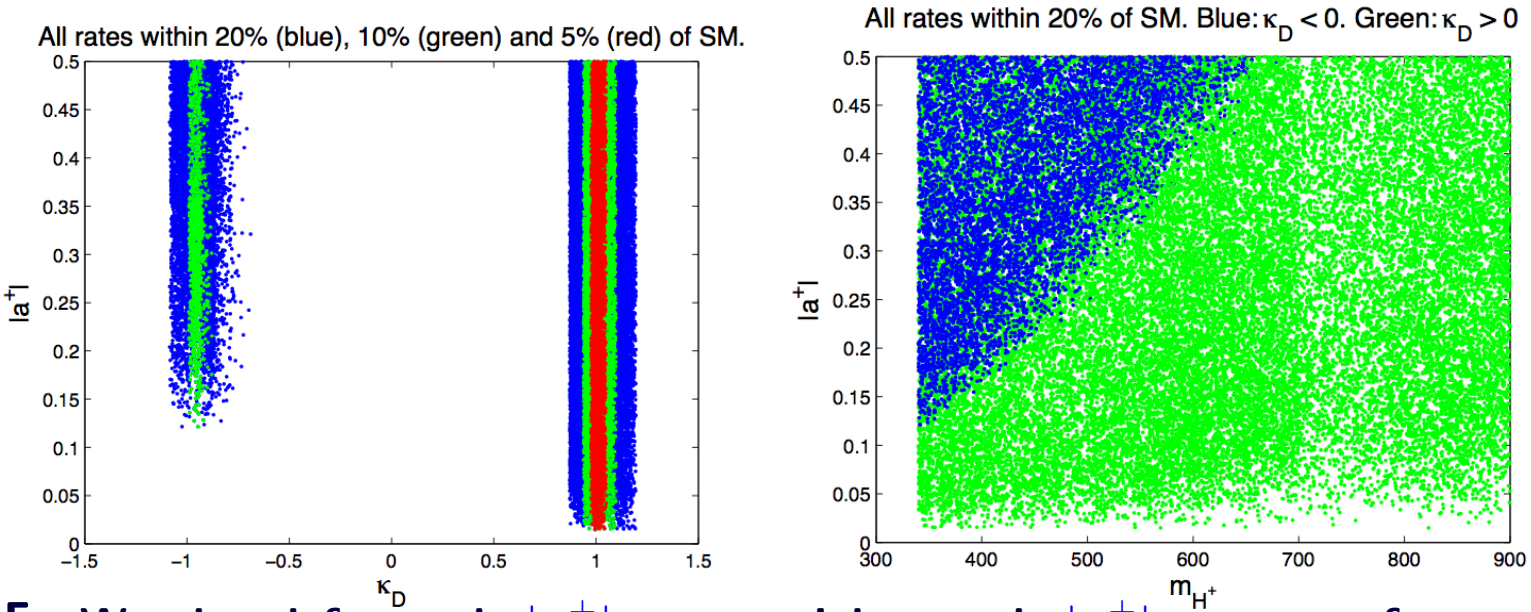

Figure 15: We plot: left panel: $|a^+|$ vs. κ_d; right panel: $|a^+|$ vs. $m_{H^\pm}$ for $\kappa_d < 0$ (blue) and $\kappa_d > 0$ (green) points with all $\mu_X^h(Y)$ within 20% of unity.

Should experiment eventually find that $\kappa_d < 0$ is preferred then we should also find $m_{H^\pm} < 650$ GeV.

- **Low-mass Higgs bosons in the 2HDM**

Let us now focus on low-$m_A < m_h/2$ points.

They are present for both Type I and Type II and have similar features in the two cases in many respects, except A production in Type I is much smaller than in Type II.

Points with acceptably small $\mathrm{BR}(h \to AA)$ exist, but it takes a highly tuned scan to find them since generically the coupling λ_{hAA} is quite large.

One must also have small $\mathrm{BR}(h \to ZA)$. However, since $g_{hZA} \propto \cos(\beta - \alpha)$, and $\cos(\beta - \alpha)$ is smallish, ZA is more easily suppressed given that the h is fairly SM-like.

Features of the surviving points are shown in Figs. 17 and 18. Note the suppression of $\mu_{gg}(\gamma\gamma)$ and that $h \to ZA$ can still be an important channel. Obviously, both should be looked for!

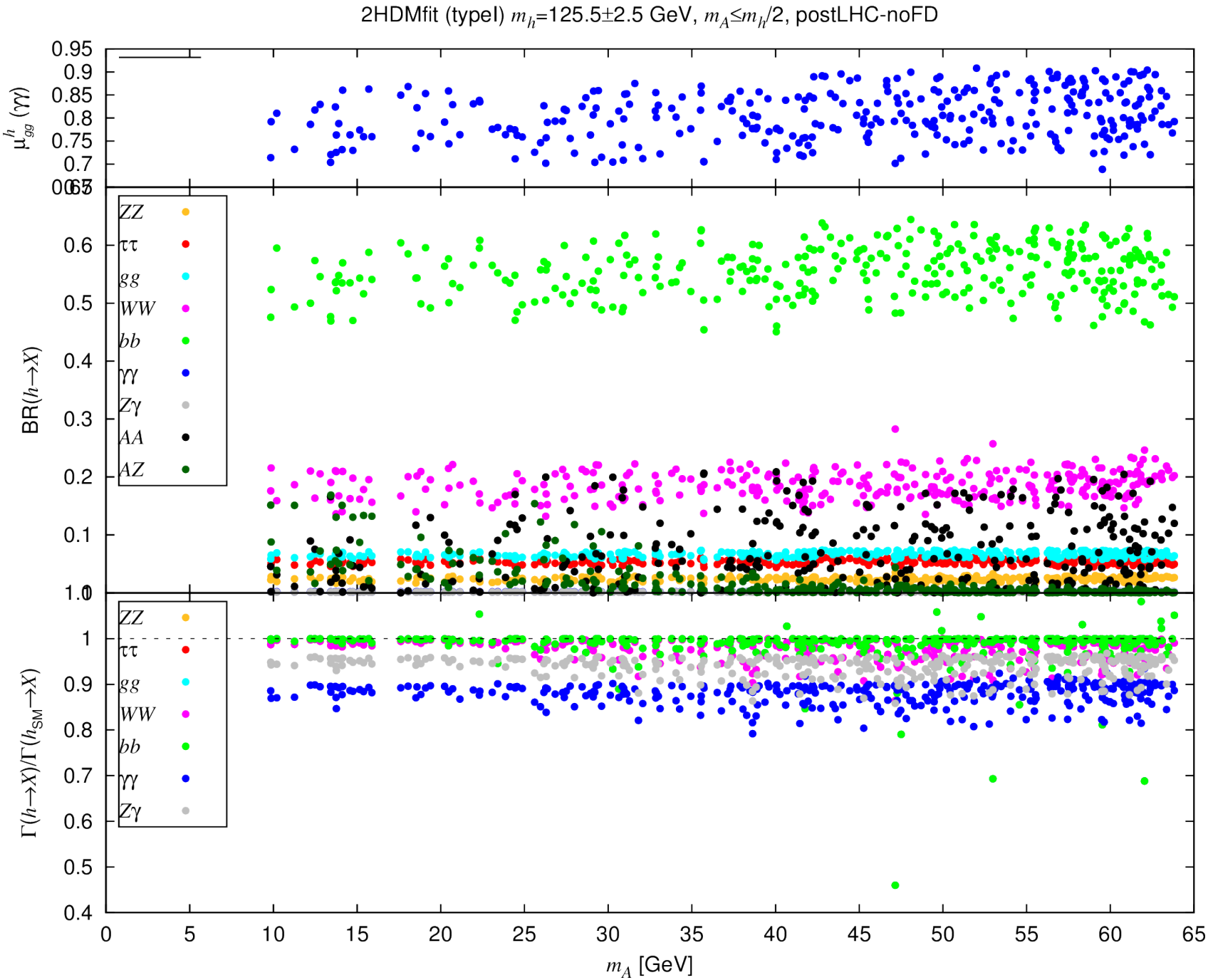

Figure 16: Features of Type-I postLHC8 points with $m_A < m_h/2$.

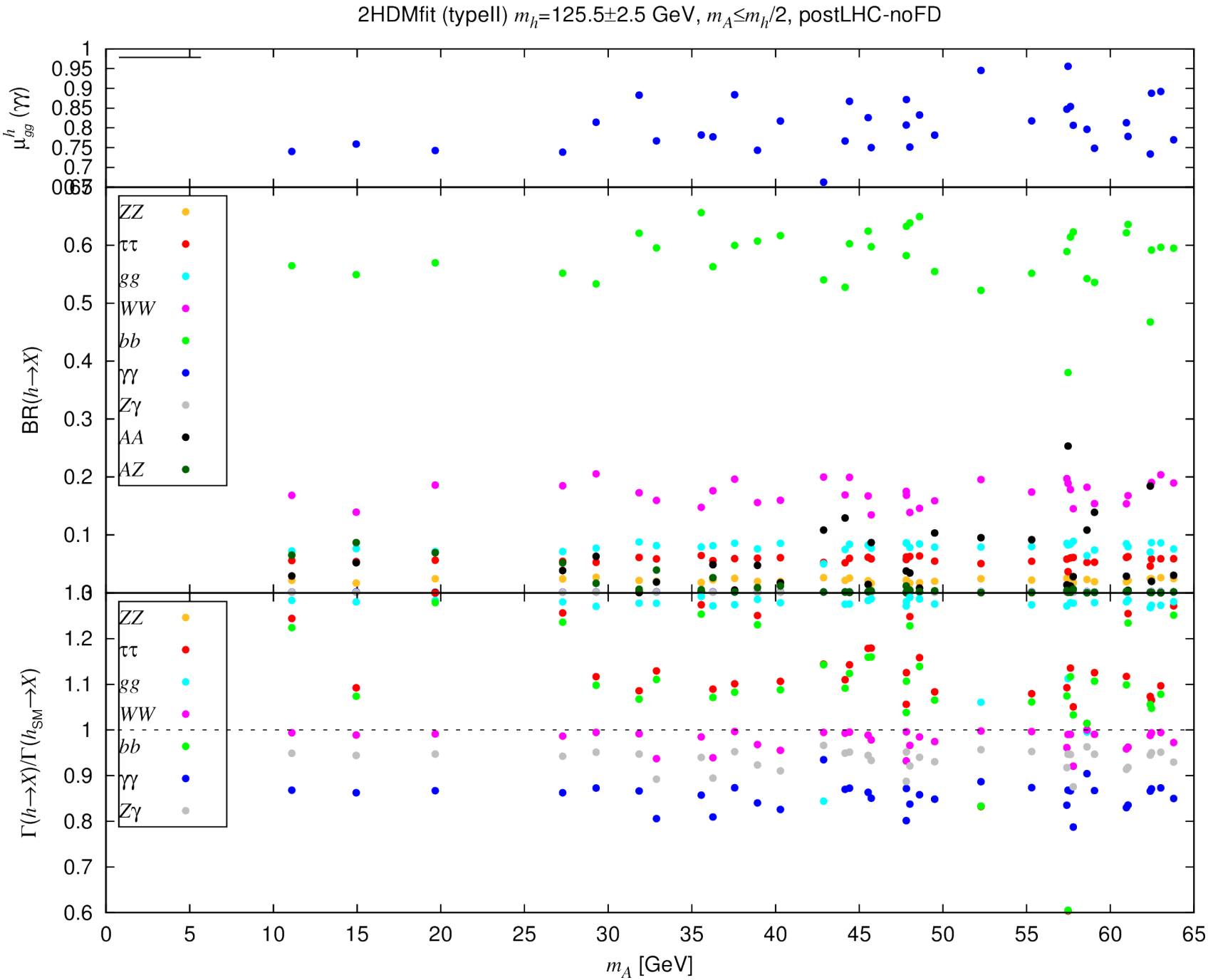

Figure 17: Features of Type-II postLHC8 points with $m_A < m_h/2$.

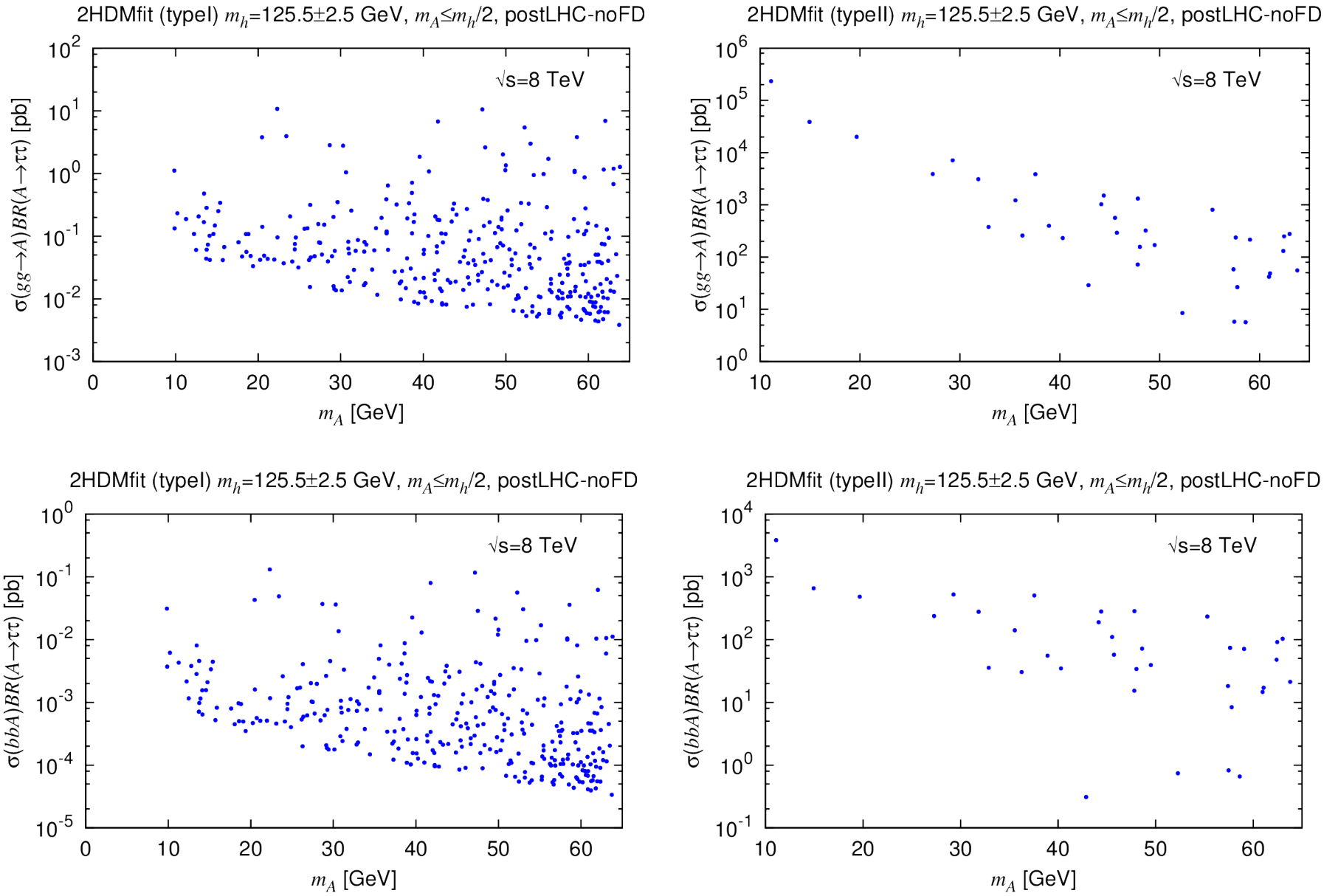

Figure 18: We plot the cross sections for $gg \to A$ and bbA with $A \to \tau\tau$ for $m_A < m_h/2$ in models of Type-I and Type-II at $\sqrt{s} = 8$ TeV. All points pass all constraints at the postLHC8 level, including $m_h = 125$ GeV higgs fitting.

Fig. 19 shows that $gg \to A$ and bbA with $A \to \tau\tau$ cross sections are very large! Spread in points comes from $\tan\beta$ variation.

Notes:
a) Even above the $b\bar{b}$ threshold $\mathrm{BR}(A \to \tau\tau) \sim 0.07$ at $m_A \sim 11$ GeV, declining to 0.045 at high $m_A \gtrsim 15$ GeV.
b) The constraints built into the Monte Carlo employed (2HDMC) are a bit naive for $m_A < 2m_b$ and so there are actually points with lower m_A that have comparable $\sigma\mathrm{BR}$ values to those shown.

Just to get a point of reference let us take $\sigma\mathrm{BR}(A \to \tau\tau) \sim 10$ pb. With 20 fb^{-1} of data, there are 2×10^5 events before cuts and efficiencies. If the net efficiency is of order 10^{-4} (which is meant to include a final mode branching ratio such as $\mathrm{BR}(\tau\tau \to \tau_\mu\tau_h) \sim 0.22$ as well as acceptance and other efficiencies, such as b-tagging), this still leaves about 20 events.

In Type I, $\sigma(gg \to A)\mathrm{BR}$ ($\sigma(bbA)\mathrm{BR}$ is much smaller) can be as large as 10 pb, but mostly lower, so hard to see anything using current data.

In Type II, both $\sigma(gg \to A)\mathrm{BR}$ and $\sigma(bbA)\mathrm{BR}$ are potentially observable. One gets the following table.

m_A(GeV)	10	20	30	40	50	60
$gg \to A$	4×10^5	4×10^4	$2000 - 8000$	$200 - 2000$	$20 - 2000$	$10 - 1000$
bbA	10000	$1000 - 2000$	$80 - 1000$	$20 - 800$	$2 - 600$	$.2 - 200$

Table 2: Very crude event number table assuming $acceptance \times efficiency \times \mathrm{BR}(\tau\tau \to mode)$ of order 10^{-4}: more scanning needed to be sure of full ranges. Efficiency will depend on whether or not there is b-tagging and acceptance will probably increase at larger m_A.

$\Rightarrow$ much of the parameter space can probably be eliminated using current data and sophisticated analyses.

Of course, there is also the $\mu\mu$ final state. There are a number of relevant CMS analyses (probably also ATLAS). Recall the CMS analysis of arXiv:1206.6326, which obtained limits of $\sigma(gg \to A)\mathrm{BR}(A \to \mu\mu) \leq 2-3$ pb for $m_A \in [11-14]$ GeV using 1.3 fb^{-1} of data. This can be compared to the predictions shown in Fig. 20.

From this, it seems that Type-II is ruled out for $m_A < 14$ GeV, but not Type-I.

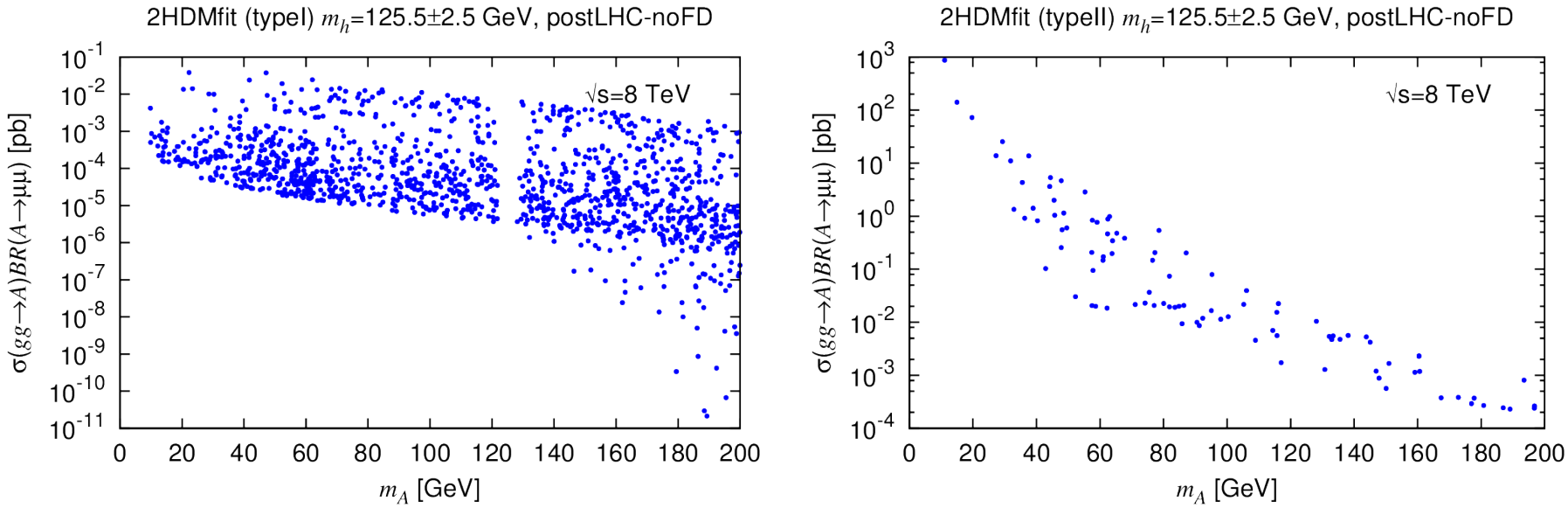

Figure 19: We plot $\sigma(gg \to A)\mathrm{BR}(A \to \mu\mu)$ for $m_A < 200$ GeV in models of Type-I and Type-II. All points pass all constraints at the postLHC8 level, including $m_h = 125$ GeV higgs fitting.

An aside: there are limits from CMS PAS HIG-13-007 of order $0.02 - 0.03$ pb for $m_A \in [100, 150]$ GeV assuming that the A and H behave similarly in the $\mu\mu$ channels as regards efficiencies and acceptance. These are not relevant for $m_A < m_h/2$, but, while the limits are not quite strong enough to impact either Type-I or Type-II, observation could be right around the corner if further analysis improvements are possible.

What happens as we move to SM$\pm 15\%, \pm 10\%, \pm 5\%$ for the $h125$? In both Type I and Type II, the $\gamma\gamma$ final state has a suppressed rate, as illustrated by plotting C_γ^h vs. m_A, see Fig. 21. For $m_A < 65$ GeV, $\kappa_\gamma \equiv C_\gamma^h \sim 0.95$, implying a 10% decrease in $\Gamma(h \to \gamma\gamma)$.

As also illustrated in Fig. 21, this comes about because of non-decoupling of the charged Higgs loop contribution to the $h\gamma\gamma$ coupling.

Recall: if $v^2 g_{hH^+H^-}/m_{H^\pm}^2 \sim -2$ then the $H^\pm$ loop is in a maximally non-decoupling regime where it cancels against the sum of the W, t and b loops and reduces C_γ^h by 5%.

This is related to the fact that most (Type I) or all (Type II) of the $m_A < m_h/2$ points have $\sin\alpha > 0$. (For Type II, but not Type I, this also implies $C_D^h < 0$.)

In the case of Type II, $\kappa_g \equiv C_g^h$ gets enhanced by 1.13 because of the change in the sign of the top-bottom interference $\Rightarrow$ easily eliminated if the Higgs rates are observed to be increasingly SM-like, as outlined earlier.

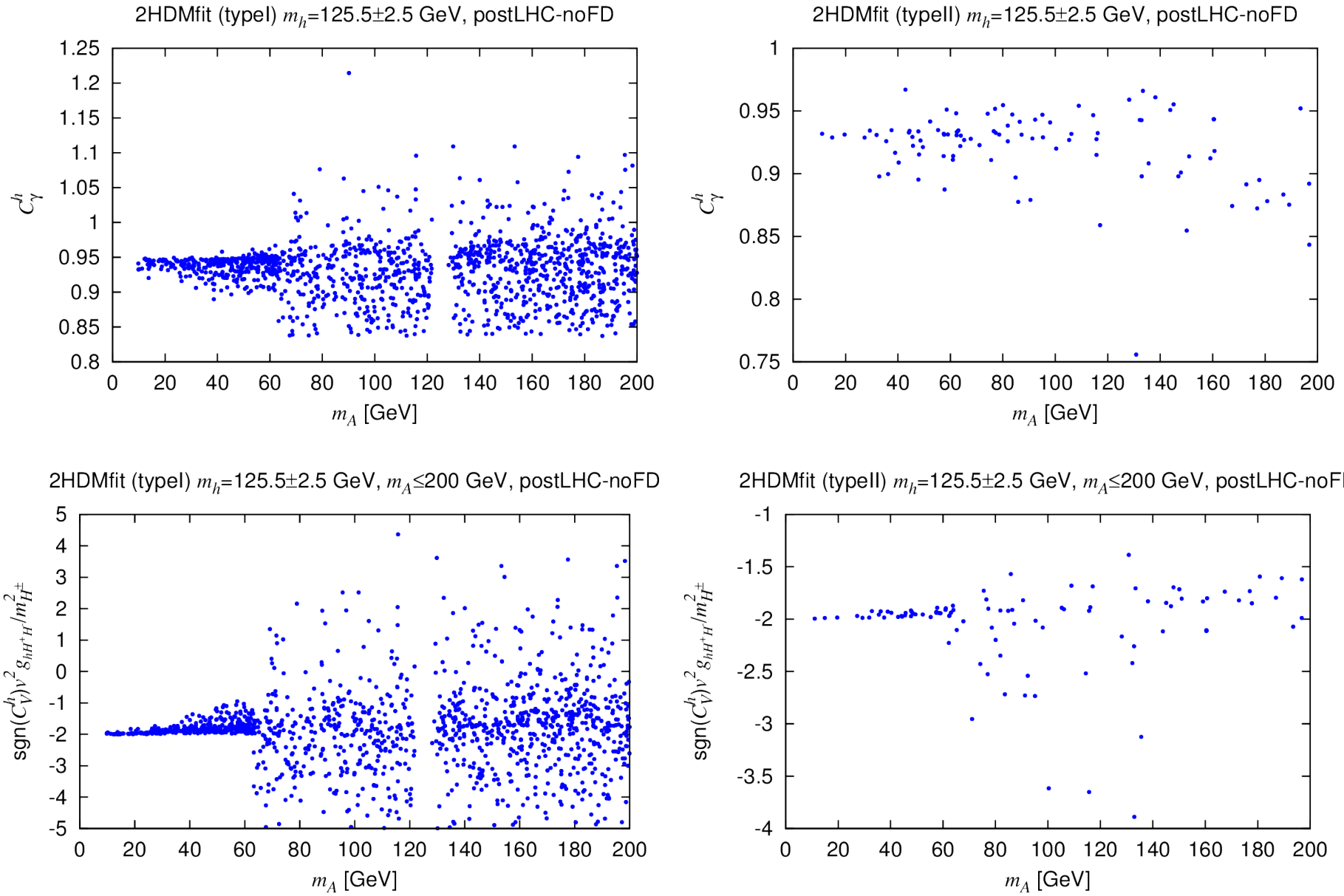

Figure 20: We plot C_γ vs. m_A (top) and $v^2 g_{hH^+H^-}/m_{H^\pm}^2$ (bottom) vs. m_A for $m_A < 200$ GeV in models of Type-I and Type-II. All points pass all constraints at the postLHC8 level, including $m_h = 125$ GeV higgs fitting.

Conclusions

- **It seems likely that the Higgs responsible for EWSB has emerged.**
- **At the moment, there is no sign of other Higgs-like signals except $\sim 1\sigma$ hints at ~ 135 GeV and the old LEP excess at 98 GeV.**
- **One may wish to focus on scenarios in which the observed Higgs is very SM-like.**
- **In models such as the 2HDM, heavier Higgs bosons may well be observable.**
- **The possibility of a light A in association with a nearly, but not quite ($\kappa_\gamma \equiv C_\gamma^h \sim 0.95$ and, for Type-II, $\kappa_g \equiv C_g^h \sim 1.13$) SM-like scalar Higgs remains open and has very interesting implications.**

  Strong signals could be present in the 8 TeV data in the case of Type-II 2HDM models.

While the waiting for a 1st Higgs signal is over, watching for more Higgs or some sign of BSM is not.